![emeraldinsight]

International Journal of Numerical Methods for Heat & Fluid Flow

Integral transform solution of natural convection in a cylinder cavity with uniform internal heat generation
Guangming Fu, Chen An, Jian Su,

Article information:

Users who downloaded this article also downloaded:

(2018),"Hybrid solutions obtained via integral transforms for magnetohydrodynamic flow with heat transfer in parallel-plate channels", International Journal of Numerical Methods for Heat & Fluid Flow, Vol. 28 Iss 7 pp. 1474-1505 https://doi.org/10.1108/HFF-02-2017-0076

(2018),"Turbulent natural convection combined with surface thermal radiation in a square cavity with local heater", International Journal of Numerical Methods for Heat & Fluid Flow, Vol. 28 Iss 7 pp. 1698-1715 https://doi.org/10.1108/HFF-03-2018-0089

For Authors

If you would like to write for this, or any other Emerald publication, then please use our Emerald for Authors service information about how to choose which publication to write for and submission guidelines are available for all. Please visit www.emeraldinsight.com/authors for more information.

About Emerald www.emeraldinsight.com

Emerald is a global publisher linking research and practice to the benefit of society. The company manages a portfolio of more than 290 journals and over 2,350 books and book series volumes, as well as providing an extensive range of online products and additional customer resources and services.

Emerald is both COUNTER 4 and TRANSFER compliant. The organization is a partner of the Committee on Publication Ethics (COPE) and also works with Portico and the LOCKSS initiative for digital archive preservation.

Integral transform solution of natural convection in a cylinder cavity with uniform internal heat generation

Guangming Fu

School of Petroleum Engineering, China University of Petroleum (East China), Qingdao, China and National Engineering Laboratory for Testing and Detection Technology of Subsea Equipment, Qingdao, China and Nuclear Engineering Program, Federal University of Rio de Janeiro, Rio de Janeiro, Brazil

Chen An

Institute for Ocean Engineering, China University of Petroleum (Beijing), Beijing, China, and

Jian Su

Nuclear Engineering Program, Federal University of Rio de Janeiro, Rio de Janeiro, Brazil

Abstract

Purpose – The purpose of this study is to propose the generalised integral transform technique to investigate the natural convection behaviour in a vertical cylinder under different boundary conditions, adiabatic and isothermal walls and various aspect ratios.

Design/methodology/approach – GITT was used to investigate the steady-state natural convection behaviour in a vertical cylinder with internal uniformed heat generation. The governing equations of natural convection were transferred to a set of ordinary differential equations by using the GITT methodology. The coefficients of the ODEs were determined by the integration of the eigenfunction of the auxiliary eigenvalue problems in the present natural convection problem. The ordinary differential equations were solved numerically by using the DBVPFD subroutine from the IMSL numerical library. The convergence was achieved reasonably by using low truncation orders.

Findings – GITT is a powerful computational tool to explain the convection phenomena in the cylindrical cavity. The convergence analysis shows that the hybrid analytical–numerical technique (GITT) has a good convergence performance in relatively low truncation orders in the stream-function and temperature fields. The effect of the Rayleigh number and aspect ratio on the natural convection behaviour under adiabatic and isothermal boundary conditions has been discussed in detail.

Originality/value – The present hybrid analytical–numerical methodology can be extended to solve various convection problems with more involved nonlinearities. It exhibits potential application to solve the convection problem in the nuclear, oil and gas industries.

Keywords Natural convection, GITT technique, Hybrid computational methodology, Vertical cylinder

Paper type Research paper

Nomenclature
C_0 = aspect ratio R/H;
$\bar{g}$ = gravitational acceleration;
H = cavity height;
k = thermal conductivity;
M_m = normalisation integral;
N_i = normalisation integral;
NT, NV = truncation order in temperature and stream-function expansions;
p = pressure;
Pr = Prandtl number;
q''' = heat generation per unit volume;
R = cylinder radius;
Ra = Rayleigh number;
T = temperature;
T_0 = temperature at the boundaries;
u = velocity component in the r-direction;
U = dimensionless velocity component in the r-direction;
U_{max} = maximum dimensionless velocity in the r-direction;
U_{min} = *minimum dimensionless velocity in the r-direction*
v = velocity component in the z-direction;
V = dimensionless velocity component in the z-direction;
V_{max} = maximum dimensionless velocity in the z-direction;
V_{min} = minimum dimensionless velocity in the z-direction;
r^*, z^* = radial and vertical coordinates;
r, z = radial and vertical coordinates, dimensionless;
X_i = eigenfunction; and
$\tilde{X}_i$ = normalised eigenfunction.

Greek Letters
α = thermal diffusivity;
β = thermal expansion coefficient;
β_m = eigenvalue;
Ω = dimensionless temperature;
$\tilde{\theta}$ = dimensionless transformed temperature;
Ω_{av} = spatially averaged dimensionless temperature;
Ω_{max} = maximum dimensionless temperature;
ϕ_m = eigenfunction;
ρ = density;
$\overline{\phi}_m$ = normalised eigenfunction;
ψ = dimensionless stream-function;
$\overline{\psi}$ = transformed stream-function;
μ_i = eigenvalue ; and
ν = kinematic viscosity.

Subscripts
i,j,m,n = eigenquantities orders

1. Introduction
The natural convection with the internal heat generation has increasingly received concerns
owing to the widely applications in the nuclear engineering and petroleum engineering. For

instance, the natural convection that occurs in closed a vertical cylinder fuel can improve the thermal efficiency through circulating the heat generation by the nuclear fuel in the reactor (Martin, 1967). The natural convection behaviours in the liquefied natural gas (LNG) storage tank laterally heated were investigated by researchers (Khelifi-Touhami *et al.*, 2010; Roh *et al.*, 2013).

Recently, the numerical and experimental methods have been widely used to investigate the natural convection in square and cylinder cavities owing to the wide applications in the actual industrial engineering (Hess and Miller, 1979; Li *et al.*, 1996; Leong, 2002; Wang *et al.*, 2014; Hu *et al.*, 2016). Fusegi *et al.* (1992) used the finite-difference numerical method to study the natural convection behaviour of the square cavity with an internal heat generation and heated on the vertical walls. Oh *et al.* (1997) studied the heat transfer behaviour and flow characteristic in natural convection with a heat-generating conducting solid in a rectangular enclosure by using the finite volume method. The adiabatic conditions on the upper and lower horizontal walls were used, while considering a temperature difference between two vertical sidewalls in their study. Rahman and Sharif (2003) adopted the finite difference method to investigate the laminar natural convection behaviour by or without considering the internal heating generation in a rectangular enclosure. El Moutaouakil *et al.* (2016) presented an analytical and numerical study to investigate the natural convection behaviour in an inclined rectangular enclosure with various aspect ratio and heated by an uniform internal volumetric heat source. Hess and Miller (1979) investigated the natural convection behaviour of vertical cylinder with a constant heat flux on the sidewall by using the experimental method. Wang *et al.* (2016) proposed a numerical methodology to study the Rayleigh–Benard natural convection with various Prandtl numbers of fluid in a vertical cylinder. Hu *et al.* (2016) performed experimental and numerical studies to investigate the Rayleigh–Benard natural convection phenomena with various aspect ratios in a vertical cylinder.

In the last decades, the hybrid analytical–numerical computational methodology (GITT) has been recognised as a powerful computational tool to explain the heat transfer and diffusion–convection phenomena (Nogueira and Cotta, 1990; Pontedeiro *et al.*, 2008; Monteiro *et al.*, 2009; Knupp *et al.*, 2014, 2015a, 2015b; Cotta *et al.*, 2016) and for the solutions of Navier–Stokes equations (Lima *et al.*, 1997; Pereira *et al.*, 1998, 2000; de Lima *et al.*, 2007; Paz *et al.*, 2007; Silva *et al.*, 2010). In the convection behaviour analysis, the GITT technique has been approved as an accurate hybrid analytical–numerical methodology (Leal *et al.*, 1999, 2000; Alves *et al.*, 2002; Neto *et al.*, 2006; Monteiro *et al.*, 2010; An *et al.*, 2013). Leal *et al.* (1999, 2000) used the GITT methodology to investigate the steady and transient convection behaviours in a steady and transient laminar flow in a square cavity, respectively. In their study, the adiabatic boundary condition on the upper surface was assumed and a temperature difference between two lateral vertical walls was used, which can induce the natural convection circulation inside the cavity. Alves *et al.* (2002) presented a stability analysis of the natural convection in porous cavities under various aspect ratios by using the GITT technique. Later, Neto *et al.* (2006) performed a study to investigate the effect of the aspect ratio on the natural convection using a three-dimensional model. Recently, the natural convection in enclosure with the uniformly distributed heat generation was investigated using the GITT technique (An *et al.*, 2013).

In the present study, a hybrid analytical–numerical computational methodology (GITT) was developed to investigate the natural convection behaviour in vertical cylinder with uniformed internal volumetric heat source. The corresponding auxiliary eigenvalue equations were defined reasonably and the eigenfunctions and eigenvalues were obtained correctly. The Prandtl number was assumed to be 0.71 in the present study. Different

boundary conditions were considered: (a) isothermal boundary condition (both the vertical and horizontal walls were isothermal); (b) adiabatic boundary condition (the vertical wall was isothermal while the upper and the lower horizontal walls were adiabatic). The results obtained by the present GITT technique show excellent convergence behaviour at relatively low truncation orders of the temperature and stream-function expansions. The temperature and velocity components (in the radial and axial directions) were discussed in detail. Finally, the effects of the Rayleigh number and aspect ratio were discussed.

2. Mathematical formulation

Considering a vertical cylinder cavity with a radius of R and height of H, containing a fluid with uniform internal heat generation q'''. The aspect ratio (C_0) is defined as $C_0 = R/H$. Two different boundary conditions are assumed: (a) adiabatic case: horizontal walls are adiabatic and lateral walls are isothermal, maintaining at temperature T_0; and (b) isothermal case: all walls are isothermal, maintaining at temperature T_0. The schematic of vertical cylinder with internal heat generation and different boundary conditions is illustrated in Figure 1.
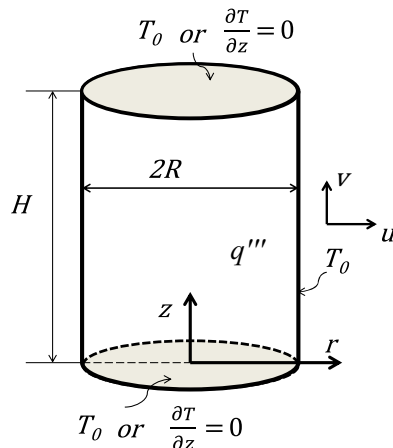
The governing equations for two-dimensional steady-state natural convection with the assumption of Boussinesq approximation in a vertical cylinder cavity can be simplified:

$$\frac{\partial u}{\partial r^*} + \frac{u}{r^*} + \frac{\partial v}{\partial z^*} = 0 \tag{1a}$$

$$\rho\left(u\frac{\partial u}{\partial r^*} + v\frac{\partial u}{\partial z^*}\right) = -\frac{\partial p}{\partial r^*} + \rho\nu\left(\nabla^2 u - \frac{u}{r^{*2}}\right) \tag{1b}$$

$$\rho\left(u\frac{\partial v}{\partial r^*} + v\frac{\partial v}{\partial z^*}\right) = -\frac{\partial p}{\partial z^*} + \rho\nu\nabla^2 v + \rho\bar{g}\beta(T - T_0) \tag{1c}$$

$$\rho c\left(u\frac{\partial T}{\partial r^*} + v\frac{\partial T}{\partial z^*}\right) = k\nabla^2 T + q''' \tag{1d}$$

Figure 1.
Schematic of vertical cylinder with internal uniformed heat generation

where r^* and z^* are, respectively, the horizontal and vertical spatial coordinates; u and v are the radial and axial velocity components, respectively; p is the pressure; T is the temperature; ρ is the density; β is the thermal expansion coefficient; $\bar{g}$ is the gravitational acceleration; c is the specific heat; and k is the thermal conductivity of the fluid.

The operator ∇^2 is described as follows:

$$\nabla^2 = \frac{1}{r^*}\frac{\partial}{\partial r^*} + \frac{\partial^2}{\partial r^{*2}} + \frac{\partial^2}{\partial z^{*2}} \tag{2}$$

The boundary conditions for the adiabatic and isothermal cases are, respectively, governed by the following:

$$\frac{\partial v}{\partial r^*} = \frac{\partial T}{\partial r^*} = 0, \ \lim_{r^* \to 0}\left[\frac{\partial \psi}{\partial r^*}\right] = 0 \quad \text{at} \quad r^* = 0 \tag{3a}$$

$$u = v = 0, \quad T = T_0 \quad \text{at} \quad r^* = R \tag{3b}$$

$$u = v = 0, \quad \frac{\partial T}{\partial z^*} = 0 \quad \text{at} \quad z^* = 0 \tag{3c}$$

$$u = v = 0, \quad \frac{\partial T}{\partial z^*} = 0 \quad \text{at} \quad z^* = H \tag{3d}$$

and

$$\frac{\partial v}{\partial r^*} = \frac{\partial T}{\partial r^*} = 0, \ \lim_{r^* \to 0}\left[\frac{\partial \psi}{\partial r^*}\right] = 0 \quad \text{at} \quad r^* = 0 \tag{4a}$$

$$u = v = 0, \quad T = T_0 \quad \text{at} \quad r^* = R \tag{4b}$$

$$u = v = 0, \quad T = T_0 \quad \text{at} \quad z^* = 0 \tag{4c}$$

$$u = v = 0, \quad T = T_0 \quad \text{at} \quad z^* = H \tag{4d}$$

The incompressible flow is assumed in the present study and the velocity components in radial and axial directions can be defined by using the stream-function ψ^*:

$$u = \frac{1}{r^*}\frac{\partial \psi^*}{\partial z^*}, \quad v = -\frac{1}{r^*}\frac{\partial \psi^*}{\partial r^*} \tag{5a, b}$$

The governing equations (1b), (1c) and (1d) can be rewritten into the following stream-function formulation:

$$\frac{1}{r^*}\frac{\partial \psi^*}{\partial z^*}\left[\frac{\partial}{\partial r^*}\left(E^2\psi^*\right) - \frac{2}{r^*}\left(E^2\psi^*\right)\right] - \frac{1}{r^*}\frac{\partial \psi^*}{\partial r^*}\frac{\partial}{\partial z^*}\left(E^2\psi^*\right)$$
$$= \upsilon\left(E^4\psi^*\right) - r^*\overline{g}\beta\frac{\partial T}{\partial r^*}$$

(6)

$$\frac{\partial^2 T}{\partial r^{*2}} + \frac{1}{r^*}\frac{\partial T}{\partial r^*} + \frac{\partial^2 T}{\partial z^{*2}} = -\frac{q'''}{k} + \frac{\rho c}{r^* k}\left(\frac{\partial \psi^*}{\partial z^*}\frac{\partial T}{\partial r^*} - \frac{\partial \psi^*}{\partial r^*}\frac{\partial T}{\partial z^*}\right)$$

(7)

In the present study, the following dimensionless variables are defined as follows:

$$r = \frac{r^*}{R}, \quad z = \frac{z^*}{H}, \quad C_0 = \frac{R}{H}, \quad \psi = \frac{\psi^*}{\alpha},$$
$$\Omega = \frac{T - T_0}{q'''R^2/k}, \quad Pr = \frac{\nu}{\alpha} = \frac{\mu c_p}{k}, \quad Ra = \frac{\beta\overline{g}q'''H^5}{\alpha\nu k}$$

(8)

where r^* and z^* identify the dimensional spatial variables, ν is the kinematic viscosity, α is the thermal diffusivity, Ra is the Rayleigh number and Pr is the Prandtl number.

Substituting the dimensionless variables into the governing equations (6) and (7), the dimensionless governing equations can be written as follows:

$$\frac{1}{rC_0^2}\frac{\partial \psi}{\partial z}\left[\frac{\partial}{\partial r}\left(E^2\psi\right) - \frac{2}{r}\left(E^2\psi\right)\right] - \frac{1}{rC_0^2}\frac{\partial \psi}{\partial r}\frac{\partial}{\partial z}\left(E^2\psi\right)$$

$$= HPr\left(E^4\psi\right) - rH^2RaPr\frac{\partial \Omega}{\partial r}$$

(9)

$$\frac{1}{C_0^2}\left(\frac{\partial^2 \Omega}{\partial r^2} + \frac{1}{r}\frac{\partial \Omega}{\partial r}\right) + \frac{\partial^2 \Omega}{\partial z^2} = -1 + \frac{1}{rC_0^2 H}\left(\frac{\partial \psi}{\partial z}\frac{\partial \Omega}{\partial r} - \frac{\partial \psi}{\partial r}\frac{\partial \Omega}{\partial z}\right)$$

(10)

where the operators E^2 and E^4 are defined as follows:

$$E^2 = \frac{1}{C_0^2}\left(\frac{\partial^2}{\partial r^2} - \frac{1}{r}\frac{\partial}{\partial r}\right) + \frac{\partial^2}{\partial z^2}$$

(11a)

$$E^4 = \frac{1}{C_0^4}\left(\frac{\partial^4}{\partial r^4} - \frac{2}{r}\frac{\partial^3}{\partial r^3} + \frac{3}{r^2}\frac{\partial^2}{\partial r^2} - \frac{3}{r^3}\frac{\partial}{\partial r}\right) -$$
$$\frac{1}{C_0^2}\left(\frac{2}{r}\frac{\partial^3}{\partial r\partial z^2} + 2\frac{\partial^4}{\partial r^2\partial z^2}\right) + \frac{\partial^4}{\partial z^4}$$

(11b)

With the following boundary conditions, for the adiabatic case:

$$\lim_{r\to 0}\frac{\partial}{\partial r}\left[\frac{1}{r}\frac{\partial \psi}{\partial r}\right] = 0, \quad \lim_{r\to 0}\left[\frac{\partial \psi}{\partial r}\right] = \frac{\partial \Omega}{\partial r} = 0 \quad \text{at} \quad r = 0$$

(12a)

$$\psi = \frac{\partial \psi}{\partial r} = 0, \quad \Omega = 0 \quad \text{at} \quad r = 1 \tag{12b}$$

$$\psi = \frac{\partial \psi}{\partial z} = 0, \quad \frac{\partial \Omega}{\partial z} = 0 \quad \text{at} \quad z = 0 \tag{12c}$$

$$\psi = \frac{\partial \psi}{\partial z} = 0, \quad \frac{\partial \Omega}{\partial z} = 0 \quad \text{at} \quad z = 1 \tag{12d}$$

and for the isothermal case:

$$\lim_{r \to 0} \frac{\partial}{\partial r} \left[\frac{1}{r} \frac{\partial \psi}{\partial r} \right] = 0, \quad \lim_{r \to 0} \left[\frac{\partial \psi}{\partial r} \right] = \frac{\partial \Omega}{\partial r} = 0 \quad \text{at} \quad r = 0 \tag{13a}$$

$$\psi = \frac{\partial \psi}{\partial r} = 0, \quad \Omega = 0 \quad \text{at} \quad r = 1 \tag{13b}$$

$$\psi = \frac{\partial \psi}{\partial z} = 0, \quad \Omega = 0 \quad \text{at} \quad z = 0 \tag{13c}$$

$$\psi = \frac{\partial \psi}{\partial z} = 0, \quad \Omega = 0 \quad \text{at} \quad z = 1 \tag{13d}$$

3. Integral transform solution

On the basis of the principles of the integral transform technique, the auxiliary eigenvalue problems from homogeneous versions of the original stream-function field and temperature problem, as shown in equations (9) and (10), were developed; secondly, the corresponding eigenvalues and eigenfunctions that satisfy the orthogonality boundary conditions are calculated; thirdly, the integral transform pairs, including transform and inverse formulas, are determined to transform the original problem of partial differential equation (PDE) into a set of ordinary differential equations (ODEs), and the corresponding coefficients are calculated, respectively. Then, the ODEs are solved by adopting the analytic or numerical computational codes, such as *Mathematica* and IMSL Library. Finally, the original problem solutions can be obtained using the developed inverse formulas.

In the present study, the following auxiliary eigenvalue problem is chosen:

$$E^4 X_i(r) = -\lambda_i^2 E^2 X_i(r) \tag{14}$$

with the following boundary conditions:

$$\lim_{r \to 0} \left[\frac{X_i(r)}{r} \right] = 0 \tag{15a}$$

$$\lim_{r \to 0} \frac{d}{dr} \left[\frac{1}{r} \frac{dX_i(r)}{dr} \right] = 0 \tag{15b}$$

$$X_i(1) = 0 \tag{15c}$$

$$\frac{dX_i(1)}{dr} = 0 \tag{15d}$$

The eigenfunctions are determined as follows:

$$X_i(r) = r^2 - \frac{rJ_1(\lambda_i r)}{J_1(\lambda_i)} \tag{16}$$

The eigenvalues (λ_i) are obtained from the following equations:

$$J_2(\lambda_i) = 0, \quad i = 1, 2, 3, \ldots \tag{17}$$

The eigenfunctions satisfy the following orthogonality properties:

$$\int_0^1 \frac{dX_i(r)}{dr} \frac{dX_j(r)}{dr} \frac{dr}{r} = -\int_0^1 X_i(r) \left[E^2 X_j(r) \right] \frac{dr}{r} = \begin{cases} 0, & i \neq j \\ N_i, & i = j \end{cases} \tag{18}$$

The N_i is calculated as follows:

$$N_i = \int_0^1 \frac{1}{r} \left[\frac{dX_i(r)}{dr} \right]^2 dr = \frac{\lambda_i^2}{2} \tag{19}$$

The normalised eigenfunction $\tilde{X}_i(r)$ is assumed as given below:

$$\tilde{X}_i(r) = \frac{X_i(r)}{N_i^{1/2}} \tag{20}$$

When using the GITT methodology to solve the PDE system, which is governed by the equations (9)-(13d), the integral transfer and inverse pairs for the stream-function field are developed as follows:

$$\overline{\psi}_i(z) = -\int_0^1 E^2 \tilde{X}_i(r) \psi(r, z) \frac{dr}{r}, \quad \text{transform} \tag{21a}$$

$$\psi(r, z) = \sum_{i=1}^{\infty} \tilde{X}_i(r) \overline{\psi}_i(z), \quad \text{inverse} \tag{21b}$$

The eigenfunctions associated with the temperatures problem are given as follows:

$$\frac{d^2 \theta_m(r)}{dr^2} + \frac{1}{r} \frac{d\theta_m(r)}{dr} = -\beta_m^2 \theta_m(r) \tag{22}$$

with the following boundary conditions:

$$\theta_m(1) = 0 \tag{23a}$$

$$\lim_{r \to 0} \left[\frac{d\theta_m(0)}{dr} \right] = 0 \tag{23b}$$

The eigenfunctions are governed as below:

$$\theta_m(r) = J_0(\beta_m r) \tag{24}$$

The eigenvalues (β_m) are computed from the following equations:

$$J_0(\beta_m) = 0, \quad m = 1, 2, 3, \ldots \tag{25}$$

The eigenfunctions satisfy the following orthogonality properties:

$$\int_0^1 r\theta_m(r)\theta_n(r) = \begin{cases} 0, & m \neq n, \\ M_m, & m = n, \end{cases} \tag{26}$$

The norm M_m is obtained as follows:

$$M_m = \frac{J_0'^2(\beta_m)}{2} \tag{27}$$

The normalised eigenfunctions are determined as follows:

$$\tilde{\theta}_m(r) = \frac{\theta_m(r)}{M_m^{1/2}} \tag{28}$$

The integral transform and inverse pairs for the temperature fields are determined as follows:

$$\overline{\phi}_m(z) = \int_0^1 r\Omega(r,z)\tilde{\theta}_m(r)dr, \quad \text{transform} \tag{29a}$$

$$\Omega(r,z) = \sum_{m=1}^{\infty} \tilde{\theta}_m(r)\overline{\phi}_m(z), \quad \text{inverse} \tag{29b}$$

The integral transformation procedure is performed through the operation of with $\int_0^1 \frac{\tilde{X}_i(r)}{r}dr$ for the stream-function field:

$$\sum_{j=1}^{\infty} A_{ij} \frac{\mathrm{d}^4 \overline{\psi}_j(z)}{\mathrm{d}z^4} - \frac{2}{C_0^{\,2}} \frac{\mathrm{d}^2 \overline{\psi}_i(z)}{\mathrm{d}z^2} + \frac{1}{C_0^{\,4}} \lambda_i^{\,2} \overline{\psi}_i(z)$$

$$= \frac{R_a}{H} \sum_{m=1}^{\infty} E_{im} \overline{\phi}_m(z) + \frac{1}{HP_r} \sum_{j=1}^{\infty} \sum_{k=1}^{\infty} \left[\frac{1}{C_0^{\,4}} B_{ijk} \overline{\psi}_j(z) \frac{\mathrm{d}\overline{\psi}_k(z)}{\mathrm{d}z} \right.$$

$$\left. + \frac{1}{C_0^{\,2}} C_{ijk} \frac{\mathrm{d}\overline{\psi}_j(z)}{\mathrm{d}z} \frac{\mathrm{d}^2 \overline{\psi}_k(z)}{\mathrm{d}z^2} + \frac{1}{C_0^{\,2}} D_{ijk} \overline{\psi}_j(z) \frac{\mathrm{d}^3 \overline{\psi}_k(z)}{\mathrm{d}z^3} \right]$$

$$i = 1, 2, 3, \dots \tag{30}$$

where the coefficients are calculated through the numerical computational packages of *Mathematica* (Wolfram, 2003):

$$A_{ij} = \int_0^1 \frac{\tilde{X}_i \tilde{X}_j}{r} \mathrm{d}r$$

$$B_{ijk} = \int_0^1 \tilde{X}_i \left(\frac{1}{r^2} \tilde{X}_j''' \tilde{X}_k - \frac{3}{r^3} \tilde{X}_j'' \tilde{X}_k + \frac{3}{r^4} \tilde{X}_j' \tilde{X}_k - \frac{1}{r^2} \tilde{X}_j' \tilde{X}_k'' + \frac{1}{r^3} \tilde{X}_j' \tilde{X}_k' \right) \mathrm{d}r$$

$$C_{ijk} = \int_0^1 \tilde{X}_i \left(\frac{1}{r^2} \tilde{X}_j \tilde{X}_k' - \frac{2}{r^3} \tilde{X}_j \tilde{X}_k \right) \mathrm{d}r$$

$$D_{ijk} = -\int_0^1 \frac{1}{r^2} \tilde{X}_i \tilde{X}_j' \tilde{X}_k \mathrm{d}r$$

$$E_{im} = \int_0^1 \tilde{X}_i \tilde{\theta}_m' \mathrm{d}r$$

$$\tag{31a, b, c, d, e}$$

Similarly, the govern equation of temperature field is operated using $\int_0^1 \tilde{\theta}_m(r) r \mathrm{d}r$, given by the following:

$$\frac{\mathrm{d}^2 \overline{\phi}_m(z)}{\mathrm{d}z^2} = \frac{1}{C_0^{\,2}} \frac{1}{H} \sum_{n=1}^{\infty} \sum_{j=1}^{\infty} \left[Q_{mnj} \overline{\phi}_n \frac{\mathrm{d}\overline{\psi}_j}{\mathrm{d}z} - S_{mnj} \frac{\mathrm{d}\overline{\phi}_n}{\mathrm{d}z} \overline{\psi}_j \right]$$

$$+ \frac{1}{C_0^{\,2}} \beta_m^2 \overline{\phi}_m - P_m \quad m = 1, 2, 3, \dots \tag{32}$$

where the associated coefficients above are the integrals of the corresponding eigenfunctions:

$$Q_{mnj} = \int_0^1 \tilde{\theta}_m \tilde{\theta}_n' \tilde{X}_j \mathrm{d}r, \qquad S_{mnj} = \int_0^1 \tilde{\theta}_m \tilde{\theta}_n \tilde{X}_j' \mathrm{d}r \tag{33a, b}$$

$$P_m = \int_0^1 r \tilde{\theta}_m \mathrm{d}r \tag{33c}$$

The coupled stream-function and temperature problems in equations (30) and (32) are constrained by the boundary conditions at two points, which are given by:

$$\overline{\psi}_i(0) = 0, \qquad \frac{\mathrm{d}\overline{\psi}_i(0)}{\mathrm{d}z} = 0, \qquad \frac{\mathrm{d}\overline{\phi}_m(0)}{\mathrm{d}z} = 0 \qquad\qquad (34\mathrm{a,\ b,\ c})$$

$$\overline{\psi}_i(1) = 0, \qquad \frac{\mathrm{d}\overline{\psi}_i(1)}{\mathrm{d}z} = 0, \qquad \frac{\mathrm{d}\overline{\phi}_m(1)}{\mathrm{d}z} = 0 \qquad\qquad (34\mathrm{d,\ e,\ f})$$

and

$$\overline{\psi}_i(0) = 0, \qquad \frac{\mathrm{d}\overline{\psi}_i(0)}{\mathrm{d}z} = 0, \qquad \overline{\phi}_m(0) = 0 \qquad\qquad (35\mathrm{a,\ b,\ c})$$

$$\overline{\psi}_i(1) = 0, \qquad \frac{\mathrm{d}\overline{\psi}_i(1)}{\mathrm{d}z} = 0, \qquad \overline{\phi}_m(1) = 0 \qquad\qquad (35\mathrm{d,\ e,\ f})$$

Finally, the convection problem is numerically solved by using a computer programme developed in Fortran 90, based on a subroutine DBVPFE in the IMSL library. The local relative error 10^{-4} is maintained automatically in the present study. The governing equations (30) and (32) are rewritten as a first-order ODE system, as shown in equation (36).

$$\mathbf{F}' = f(\mathbf{F}, z) \qquad\qquad (36)$$

Truncation order	Ra = 3,900			Ra = 10,000		
	$\Omega(0.25, 0.5)$	$U(0.5, 0.25)$	$V(0.25, 0.5)$	$\Omega(0.25, 0.5)$	$U(0.5, 0.25)$	$V(0.25, 0.5)$
NV = 4, NT = 4	0.019048	−0.273714	0.493233	0.019045	−0.697076	1.262815
NV = 4, NT = 10	0.019044	−0.273713	0.493139	0.019041	−0.697073	1.262576
NV = 4, NT = 20	0.019044	−0.273713	0.493139	0.019041	−0.697073	1.262576
NV = 8, NT = 8	0.019044	−0.276622	0.477352	0.019041	−0.704393	1.222159
NV = 10, NT = 10	0.019044	−0.277109	0.480554	0.019041	−0.705618	1.230355
NV = 20, NT = 4	0.019048	−0.277092	0.480626	0.019045	−0.705571	1.230535
NV = 20, NT = 20	0.019044	−0.277089	0.480549	0.019041	−0.705563	1.230337
	$\Omega(0.5, 0.5)$	$U(0.5, 0.5)$	$V(0.5, 0.5)$	$\Omega(0.5, 0.5)$	$U(0.5, 0.5)$	$V(0.5, 0.5)$
NV = 4, NT = 4	0.014513	−0.003465	0.171135	0.014511	−0.022678	0.439195
NV = 4, NT = 10	0.014517	−0.003465	0.171188	0.014517	−0.022675	0.452072
NV = 4, NT = 20	0.014517	−0.003465	0.171188	0.014515	−0.022675	0.452072
NV = 8, NT = 8	0.014517	−0.003574	0.175184	0.014515	−0.023391	0.449531
NV = 10, NT = 10	0.014517	−0.003588	0.176518	0.014515	−0.023485	0.452942
NV = 20, NT = 4	0.014513	−0.003591	0.176178	0.014511	−0.023503	0.452072
NV = 20, NT = 20	0.014517	−0.003590	0.176231	0.014515	−0.023499	0.452207
	$\Omega(0.75, 0.5)$	$U(0.5, 0.75)$	$V(0.75, 0.5)$	$\Omega(0.75, 0.5)$	$U(0.5, 0.75)$	$V(0.75, 0.5)$
NV = 4, NT = 4	0.007689	0.275713	−0.213701	0.007688	0.710129	−0.547559
NV = 4, NT = 10	0.007686	0.275712	−0.213742	0.007685	0.710125	−0.547665
NV = 4, NT = 20	0.007686	0.275712	−0.213742	0.007685	0.710125	−0.547665
NV = 8, NT = 8	0.007685	0.278684	−0.193557	0.007684	0.717859	−0.495881
NV = 10, NT = 10	0.007686	0.279181	−0.197421	0.007685	0.719154	−0.505787
NV = 20, NT = 4	0.007689	0.279164	−0.195847	0.007688	0.719108	−0.501752
NV = 20, NT = 20	0.007686	0.279161	−0.195906	0.007685	0.719099	−0.501902

Table I.
Convergence analysis with isothermal wall conditions when $C_0 = 1$ and Pr = 0.71

where **F** is defined as follows:

$$\mathbf{F} = \left\{ \bar{\psi}_1, \frac{\mathrm{d}\overline{\psi}_1}{\mathrm{d}z}, \frac{\mathrm{d}^2\overline{\psi}_1}{\mathrm{d}z^2}, \frac{\mathrm{d}^3\overline{\psi}_1}{\mathrm{d}z^3}, \ldots, \overline{\psi}_{NV}, \frac{\mathrm{d}\overline{\psi}_{NV}}{\mathrm{d}z}, \right.$$
$$\left. \frac{\mathrm{d}^2\overline{\psi}_{NV}}{\mathrm{d}z^2}, \frac{\mathrm{d}^3\overline{\psi}_{NV}}{\mathrm{d}z^3}, \overline{\phi}_1, \frac{\mathrm{d}\overline{\phi}_1}{\mathrm{d}z}, \ldots, \overline{\phi}_{NT}, \frac{\mathrm{d}\overline{\phi}_{NT}}{\mathrm{d}z} \right\}^{\mathrm{T}} \qquad (37)$$

Here, NV and NT are the reasonable truncation orders that assure a sufficient convergence requirement for the present problem. When $\bar{\psi}_i$ and $\bar{\theta}_m$ have been numerically evaluated under the assumed accuracy, the stream-function $\psi(r, z)$ and temperature $\Omega(r, z)$ can be obtained by using the inverse formula equations (21b) and (29b). The velocity components $u(r, z)$ and $v(r, z)$ in the r and z directions, respectively, are analytically calculated based on the inversion formula and the initial definitions in the form:

$$U = \sum_{i=1}^{NV} \frac{1}{r}\tilde{X}_i(r)\frac{\mathrm{d}\overline{\psi}_i(z)}{\mathrm{d}z}, \qquad V = -\sum_{i=1}^{NV} \frac{1}{r}\frac{\mathrm{d}\tilde{X}_i(r)}{\mathrm{d}r}\overline{\psi}_i(z) \qquad (38a,\ b)$$

4. Results and discussion

4.1 Convergence analysis
In the present investigation, the Prandtl number (Pr) is assumed as 0.71, and the Rayleigh numbers are determined as Ra = 1,000, 2,000, 3,900, 8,000, 10,000, 15,000 and 30,000, respectively. In the parametric study, the aspect ratios ($C_0 = R/H$) are assumed as 0.2, 1 and
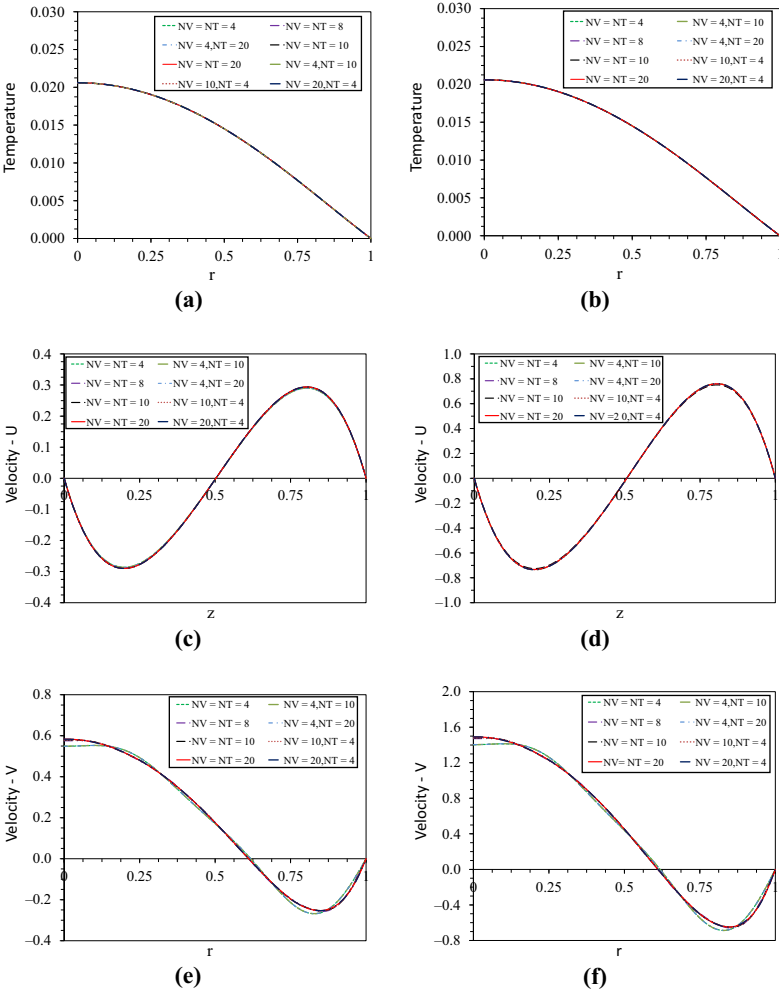
Truncation order	Ra = 3,900			Ra = 10,000		
	$\Omega(0.25, 0.5)$	$U(0.5, 0.25)$	$V(0.25, 0.5)$	$\Omega(0.25, 0.5)$	$U(0.5, 0.25)$	$V(0.25, 0.5)$
NV = 4, NT = 4	0.043020	−0.699887	1.299742	0.042945	−1.755179	3.296841
NV = 4, NT = 10	0.043016	−0.699885	1.299648	0.042941	−1.755177	3.296604
NV = 4, NT = 20	0.043016	−0.699885	1.299648	0.042941	−1.755177	3.296604
NV = 8, NT = 8	0.043016	−0.705959	1.262187	0.042940	−1.769796	3.201573
NV = 10, NT = 10	0.043016	−0.706876	1.269661	0.042940	−1.772010	3.220518
NV = 20, NT = 4	0.043020	−0.706903	1.269714	0.042943	−1.772042	3.220568
NV = 20, NT = 20	0.043016	−0.706899	1.269636	0.042940	−1.772036	3.220371
	$\Omega(0.5, 0.5)$	$U(0.5, 0.5)$	$V(0.5, 0.5)$	$\Omega(0.5, 0.5)$	$U(0.5, 0.5)$	$V(0.5, 0.5)$
NV = 4, NT = 4	0.032213	−0.023442	0.432597	0.032161	−0.149117	1.114849
NV = 4, NT = 10	0.032217	−0.023441	0.432651	0.032165	−0.149107	1.114985
NV = 4, NT = 20	0.032217	−0.023441	0.432651	0.032165	−0.149107	1.114985
NV = 8, NT = 8	0.032217	−0.024133	0.442123	0.032164	−0.153654	1.138428
NV = 10, NT = 10	0.032217	−0.024223	0.445235	0.032164	−0.154239	1.146247
NV = 20, NT = 4	0.032213	−0.024236	0.444527	0.032160	−0.154313	1.144466
NV = 20, NT = 20	0.032217	−0.024234	0.444580	0.032163	−0.154301	1.144600
	$\Omega(0.75, 0.5)$	$U(0.5, 0.75)$	$V(0.75, 0.5)$	$\Omega(0.75, 0.5)$	$U(0.5, 0.75)$	$V(0.75, 0.5)$
NV = 4, NT = 4	0.016661	0.712618	−0.560326	0.016637	1.834809	−1.428404
NV = 4, NT = 10	0.016658	0.712616	−0.560368	0.016633	1.834805	−1.428510
NV = 4, NT = 20	0.016658	0.712616	−0.560368	0.016633	1.834805	−1.428510
NV = 8, NT = 8	0.016658	0.719028	−0.512357	0.016633	1.851696	−1.305017
NV = 10, NT = 10	0.016658	0.719994	−0.521379	0.016633	1.854239	−1.328078
NV = 20, NT = 4	0.016661	0.720026	−0.517780	0.016636	1.854289	−1.318882
NV = 20, NT = 20	0.016658	0.720022	−0.517839	0.016633	1.854280	−1.319034

Table II.
Convergence analysis with adiabatic wall condition when C_0 = 1 and Pr = 0.71

2, respectively. Both the isothermal and adiabatic boundary conditions are considered in the present study. All of the cases are discussed under the axisymmetric assumption.

The convergence behaviours of the presented hybrid numerical–analytical technique (GITT) under the isothermal and adiabatic boundary conditions are investigated first when $Ra = 3,900$ and $Ra = 10,000$. Tables I and II illustrate the convergence behaviour of temperature, radial and axial velocities at various points under isothermal and adiabatic boundary conditions, respectively. The temperature and velocity variations along the r direction when $z = 0.5$ (for temperature and axial

Figure 2.
The convergence behaviour when $Pr = 0.71$ and $C_0 = 1$, using various truncation orders in isothermal conditions

Notes: The temperature when (a) Ra = 3,900; (b) Ra = 10,000; the radial velocity when; (c) Ra = 3,900; (d) Ra = 10,000; the axial velocity when (e) Ra = 3,900; (f) Ra = 10,000

velocity distributions) and z direction when $r = 0.5$ (for radial velocity distribution) are shown in Figures 2 and 3. It is noted that the temperature is converged faster in both cases of the isothermal and adiabatic conditions when $Ra = 3,900$ and $Ra = 10,000$, which is owing to that the temperature is assumed as the expansion of the original eigenfunctions, as described in equation (29), while the velocity components are defined as the first derivatives of the stream-functions [equation (38)].

The temperature converges very well with a low truncation orders ($NV = NT = 4$). The radial and axial velocities converge better with the increasing of the truncation orders, as
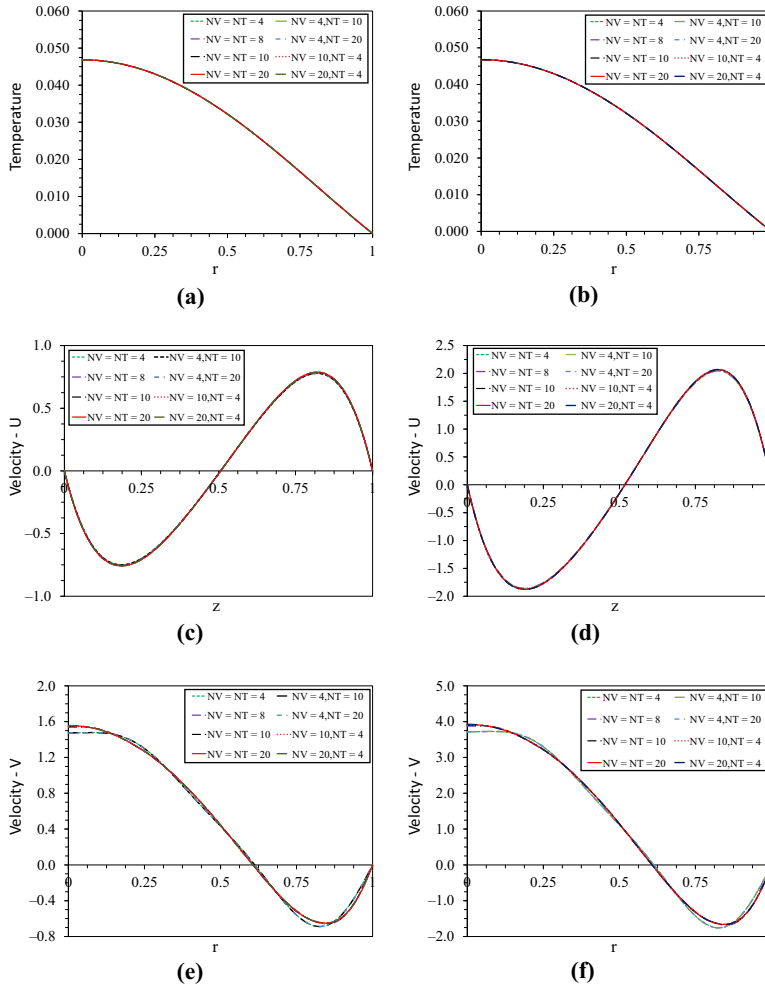
Notes: The temperature when (a) Ra = 3,900; (b) Ra = 10,000; the radial velocity when (c) Ra = 3,900; (d) Ra = 10,000; and the axial velocity when (e) Ra = 3,900; (f) Ra = 10,000

Figure 3.
The convergence analysis when Pr = 0.71 and C_0 = 1, using various truncation orders under adiabatic horizontal wall conditions

shown in Figures 2 and 3 and Tables I and II. The results show that the present hybrid analytical–numerical technique (GITT methodology) can be converged quickly at relatively low truncation orders.

Figures 4 and 5 show the contours of the dimensionless temperature, stream-function, radial and axial velocities under isothermal boundary conditions when $Ra = 10,000$ is adopted. Only one roll is observed in the present axisymmetric model both for the isothermal and adiabatic cases. The stream-function and velocity components have the similar distributions mode in the isothermal and adiabatic cases.

In case of isothermal boundary conditions, the maximum temperature occurs in the centre of the cylinder and the minimum temperature is observed around the lateral and horizontal walls [see Figure 4(a)]. However, in the case of adiabatic condition, the maximum temperature happens on the top of the vertical centreline and decreases along the r direction. The minimum temperature has uniformed distribution on the lateral wall, as shown in Figure 4(a).

The natural convection happens owing to the non-uniform distribution of the temperature and the single counter-rotating roll is observed, as shown in Figures 4(b) and 5 (b). In both cases of isothermal and adiabatic conditions, owing to the occurrence of the maximum temperature in the centreline and the minimum temperature near the vertical
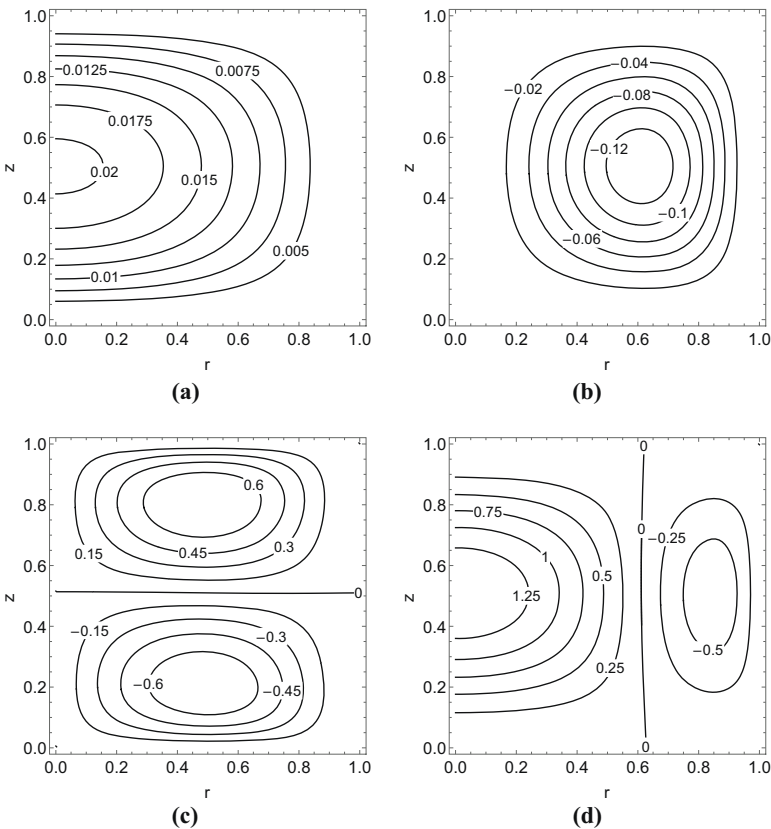
Figure 4.
Contour plots for an internally heated vertical cylinder with isothermal walls ($Ra = 10,000$, $C_0 = 1$ and $Pr = 0.71$)

Notes: (a) Temperature; (b) Streamline; (c) Radial velocity; (d) Axial velocity
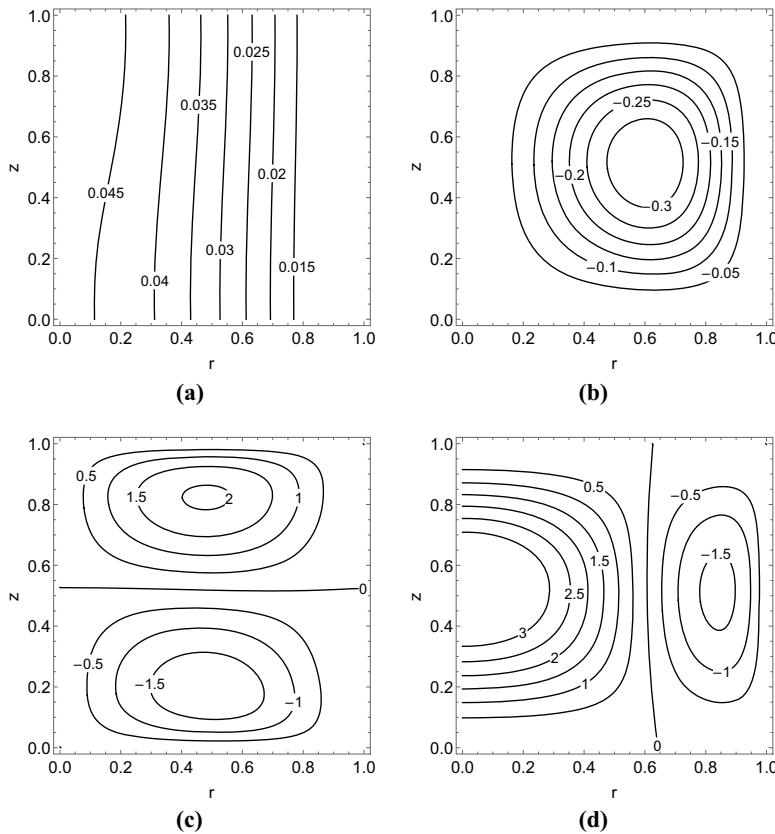
Notes: (a) temperature; (b) streamline; (c) radial velocity; (d) axial velocity

Figure 5.
Contour plots for an
internally heated
vertical cylinder with
adiabatic walls
(Ra = 10,000, $C_0 = 1$
and $Pr = 0.71$)

wall, the up-flow along the axial of the cylinder appears and the higher axial velocity
happens in this region. With the decreasing of the temperature along the r direction, the
driven force is induced by the convection decreasing and the down-flow can be observed
when the $r > 0.6$, as shown in Figures 4(d) and 5(d). Moreover, the maximum absolute
magnitude of axial velocity in the down-flow is approximately half of the corresponding
value of the up-flow in the centre, as shown in Figure 2.

4.2 Effects of Rayleigh number Ra

The aspect ratio of height to radius of $C_0 = 1$ and the Prandtl number $Pr = 0.71$ are
maintained in this section. Both the isothermal and the adiabatic boundary condition are
considered. The Rayleigh number varies from 1,000 to 30,000 for the isothermal case, and
the maximum Rayleigh number is assumed as 15,000 for the adiabatic case.

Figures 6 and 7 indicate the result comparisons under different Rayleigh number with
the isothermal and adiabatic boundaries, respectively. With the increasing of the Rayleigh
number, the absolute values of stream-function, radial and axial velocities increase linearly
for both the isothermal [as shown in Figures 6(b), (c) and (d)] and adiabatic conditions [as

Figure 6.
The comparisons of the temperature, velocities and the streamline distributions under various Rayleigh number under isothermal conditions $(Pr = 0.71, C_0 = 1)$
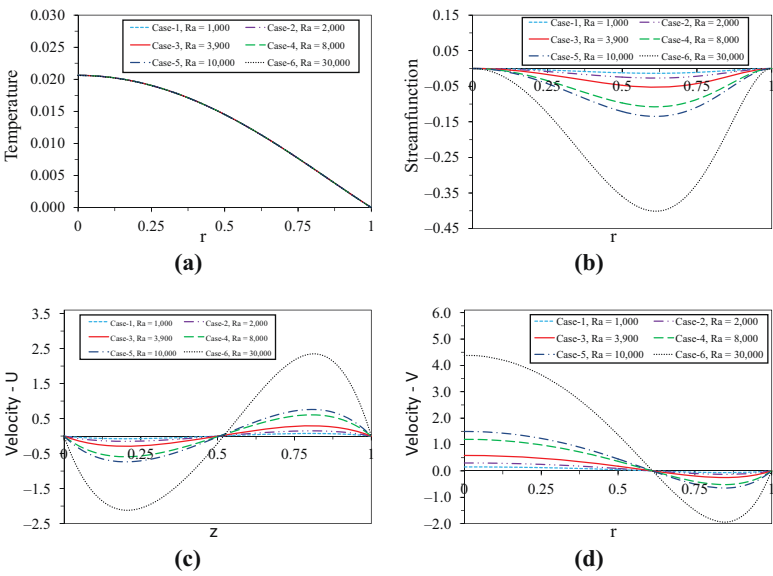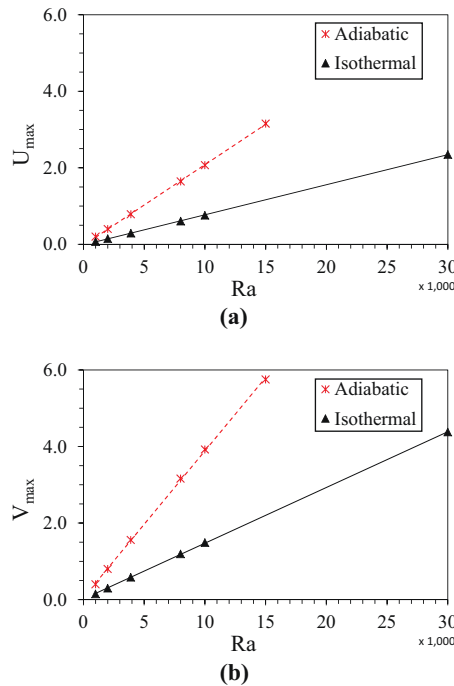
Notes: (a) Temperature at $z = 0.5$; (b) streamline at $z = 0.5$; (c) radial velocity at $r = 0.5$; (d) axial velocity at $z = 0.5$

Figure 7.
The comparisons of the temperature, velocities and the streamline distributions under various Ra number under adiabatic conditions $(Pr = 0.71, C_0 = 1)$
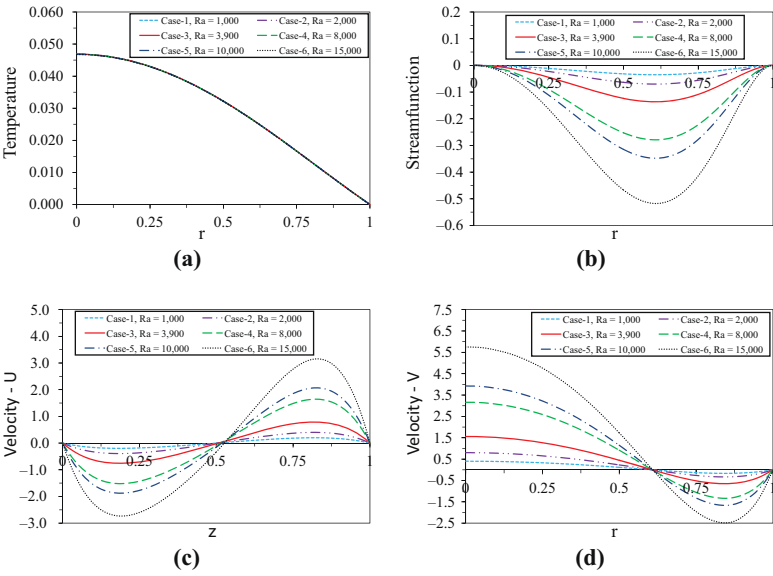
Notes: (a) Temperature at $z = 0.5$; (b) streamline at $z = 0.5$; (c) radial velocity at $r = 0.5$; (d) axial velocity at $z = 0.5$

illustrated in Figures 7(b), (c) and (d)]. Moreover, it increases more quickly in the adiabatic condition. From Figures 6(a) and (b), it can be concluded that the effects of Rayleigh number on the temperature are insignificant.

Figures 8(a) and (b) show the comparisons of the maximum radial and axial velocities with various Rayleigh numbers under the adiabatic and isothermal boundary conditions. With the increasing of the Rayleigh number, both the peak radial and axial velocities increase linearly. The maximum axial velocity is approximate as twice of the radial velocity when a constant Rayleigh number is maintained. This behaviour can be observed in both adiabatic and isothermal conditions. When the Rayleigh number is assumed as a constant, it can be observed that the maximum magnitudes of axial and radial velocities under adiabatic condition are approximate as 2.6 times of the corresponding values when all the walls are assumed as isothermal condition [see Figures 8(a) and (b)], which is owing to the higher energy is maintained under the adiabatic boundary conditions. However, in the square cavity natural convection analysis, the velocity magnitudes under adiabatic condition are twice as the ones under the isothermal condition captured by Joshi *et al.* (2006) and An *et al.* (2013).

4.3 Effects of aspect ratio $C_0 = R/H$

In the parametric study of the aspect ratio effects on natural convection behaviour, the Rayleigh number (Ra) and Prandtl number (Pr) are maintained as 2,000 and 0.71, respectively. Three aspect ratios of radius to height are assumed as $C_0 = 0.2$, $C_0 = 1$ and $C_0 = 2$, in both the isothermal and adiabatic boundary conditions.

Figure 8.
The maximum velocity components variation when different Rayleigh numbers were used

Notes: (a) Radial velocity; (b) axial velocity

Tables III and IV show the temperature and the maximum magnitude of velocity components and the corresponding coordinates. We can see that the absolute values of the temperature and velocity increase with the increasing of the aspect ratio. In the adiabatic condition, the maximum magnitudes of the radial and axial velocities are increased more quickly than the corresponding velocity in the isothermal condition.

When the aspect ratio is assumed as 2.0, the axial velocity magnitude in the down-flow is higher than the one in the up-flow under the isothermal condition, as shown in Figure 9(i). However, in the adiabatic condition, the maximum axial velocity in the up-flow is higher than the maximum velocity in the down-flow. The corresponding coordinates of maximum axial velocity are moving to the right side with the increasing of the aspect ratio both in the isothermal and adiabatic conditions, as shown in Figures 9 and 10.

5. Conclusions

A hybrid analytical–numerical computational model (GITT) was developed to investigate the natural convection behaviour in vertical cylinder with uniformed internal volumetric heat source. The results show good convergence behaviour under lower truncation orders and the computational costs were reduced significantly. The effects of the Rayleigh number and the aspect ratio on the temperature and velocity components were discussed under the isothermal and adiabatic boundary conditions. The following main conclusions can be drawn:

The convergence analysis shows that the present hybrid analytical–numerical technique (GITT) has a good convergence performance in relatively low truncation orders in the stream-function and temperature fields.

	$C_0 = 0.2$	$C_0 = 1$	$C_0 = 2$
U_{max}	0.000607	0.150	0.220085
(r, z)	(0.4475, 0.94)	(0.4875, 0.8025)	(0.6275, 0.7875)
U_{min}	−0.000607	−0.149	−0.21949
(r, z)	(0.4475, 0.0575)	(0.49, 0.1975)	(0.6275, 0.2125)
V_{max}	0.000688	0.29934	0.282041
(r, z)	(0, 0.5)	(0, 0.5025)	(0.0575, 0.5025)
V_{min}	−0.00022	−0.13022	−0.300941
(r, z)	(0.805, 0.475)	(0.8475, 0.50)	(0.905, 0.50)
Ω_{max}	0.001866	0.020615	0.028032
(r, z)	(0, 0.5)	(0,0.5)	(0, 0.5)
Ω_{av}	0.000969	0.00886	0.01214

Table III.
The axial velocity, radial velocity, temperature and their coordinates under $Pr = 0.71$ and Ra = 2,000 and isothermal wall conditions

Table IV.
The axial velocity, radial velocity, temperature and their coordinates under $Pr = 0.71$ and Ra = 2,000 and adiabatic wall conditions

|	$C_0 = 0.2$	$C_0 = 1$	$C_0 = 2$
U_{max}	0.000850	0.401065	1.723981
(r, z)	–	(0.485, 0.8175)	(0.5975, 0.7975)
V_{max}	0.000694	0.800445	2.473740
(r, z)	–	(0, 0.505)	(0.0525, 0.5125)
Ω_{max}	0.001875	0.047091	0.189781
(r, z)	–	(0, 1)	(0, 1)
Ω_{av}	0.001166	0.029151	0.116472
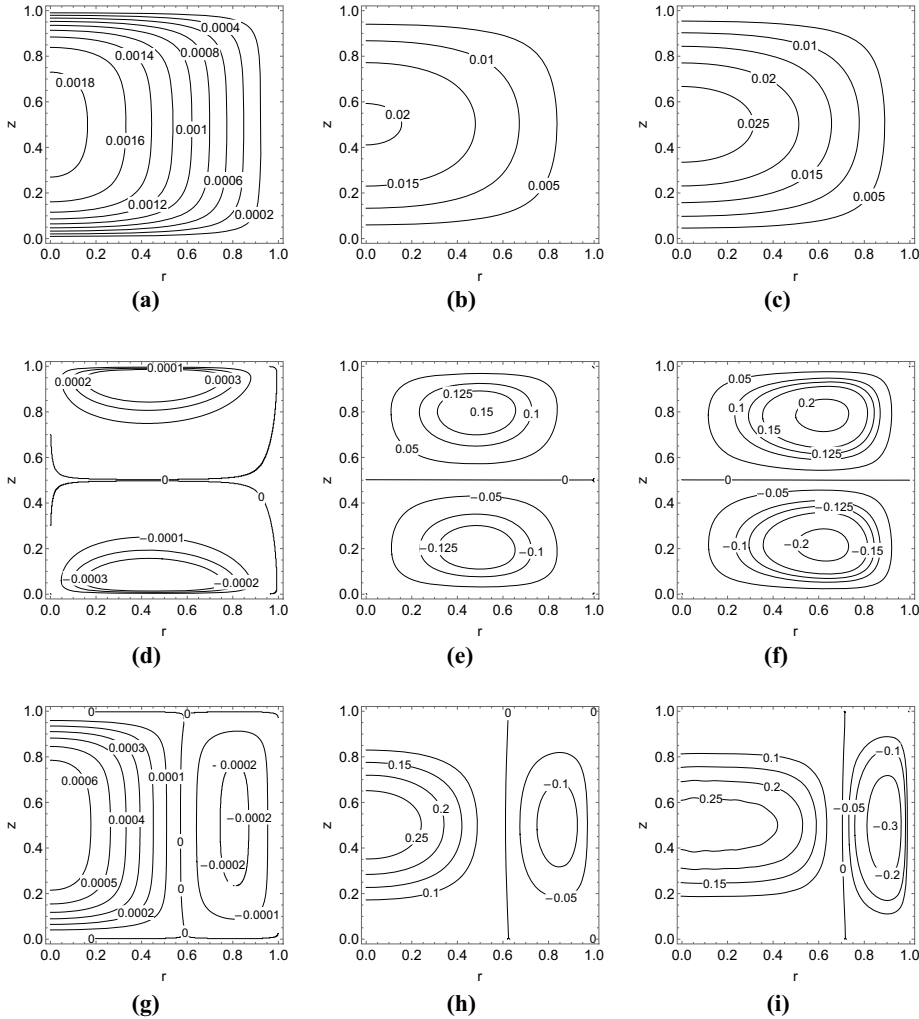
Figure 9.
The comparisons of
the results when
Pr = 0.71 and
Ra = 3,900 with
isothermal
conditions, under
various ratio of
C_0 = R/H, the
temperature when (a)
C_0 = 0.2, (b) C_0 = 1
and (c) C_0 = 2; radial
velocity (u) when (d)
C_0 = 0.2, (e) C_0 = 1
and (f) C_0 = 2; and
axial velocity (v)
when (g) C_0 = 0.2, (h)
C_0 = 1 and (i) C_0 = 2

The temperature, axial and radial velocities were calculated under the isothermal and
adiabatic boundary conditions. It is noted that the distribution mode of the velocity
components is similar. However, in the adiabatic condition, the maximum velocity
component values are 2.6 times the corresponding value in the isothermal condition.

The Rayleigh number has significant effects on the velocity components, both in the
isothermal and adiabatic boundary conditions. With the increasing of the Rayleigh number,
the radial and axial velocities increase linearly. Moreover, the velocity components increase
more quickly in the adiabatic boundary condition. The effects of the Rayleigh number on the
temperature distribution are insignificant.

The aspect ratio of radius to height has significant effects on the velocity components,
especially under the adiabatic boundary condition. With the increase in the aspect ratio, the
zero velocity region moves to the right side.
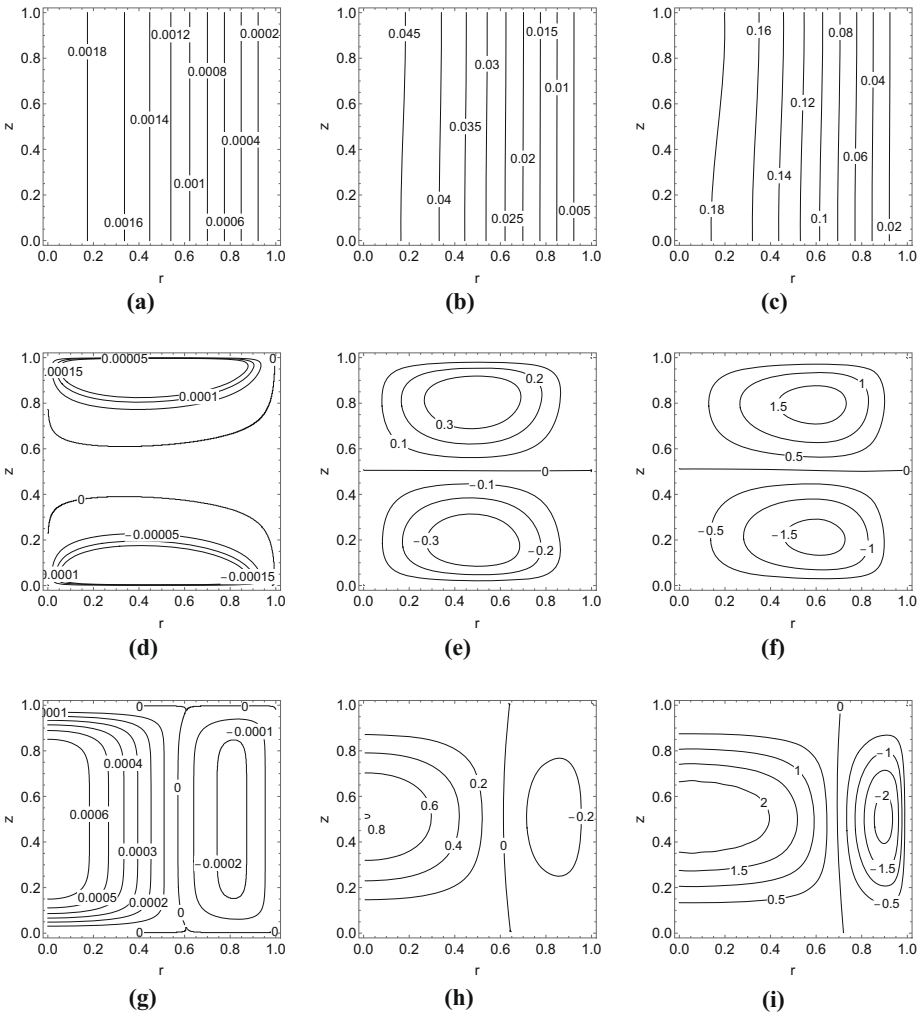
Figure 10.
The comparisons of the results when Pr = 0.71 and Ra = 2,000 with adiabatic conditions, under various ratio of C_0 = R/H, the temperature when (a) C_0 = 0.2, (b) C_0 = 1 and (c) C_0 = 2; radial velocity (u) when (d) C_0 = 0.2, (e) C_0 = 1 and (f) C_0 = 2; and axial velocity (v) when (g) C_0 = 0.2, (h) C_0 = 1 and (i) C_0 = 2

References

Alves, L.S.D., Cotta, R.M. and Pontes, J. (2002), "Stability analysis of natural convection in porous cavities through integral transforms", *International Journal of Heat and Mass Transfer*, Vol. 45 No. 6, pp. 1185-1195.

An, C., Vieira, C.B. and Su, J. (2013), "Integral transform solution of natural convection in a square cavity with volumetric heat generation", *Brazilian Journal of Chemical Engineering*, Vol. 30 No. 4, pp. 883-896.

Cotta, R.M., Naveira-Cotta, C.P. and Knupp, D.C. (2016), "Nonlinear eigenvalue problem in the integral transforms solution of convection-diffusion with nonlinear boundary conditions", *International Journal of Numerical Methods for Heat & Fluid Flow*, Vol. 26 Nos 3/4, pp. 767-789.

de Lima, G.G.C., Santos, C.A.C., Haag, A. and Cotta, R.M. (2007), "Integral transform solution of internal flow problems based on Navier-stokes equations and primitive variables formulation", *International Journal for Numerical Methods in Engineering*, Vol. 69 No. 3, pp. 544-561.

El Moutaouakil, L., Zrikem, Z. and Abdelbaki, A. (2016), "Analytical and numerical study of natural convection induced by a volumetric heat generation in inclined cavities asymmetrically cooled by heat fluxes", *Applied Mathematical Modelling*, Vol. 40 No. 4, pp. 2913-2928.

Fusegi, T., Hyun, J.M. and Kuwahara, K. (1992), "Natural-convection in a differentially heated square cavity with internal heat-generation", *Numerical Heat Transfer Part a-Applications*, Vol. 21 No. 2, pp. 215-229.

Hess, C. and Miller, C. (1979), "Natural convection in a vertical cylinder subject to constant heat flux", *International Journal of Heat and Mass Transfer*, Vol. 22 No. 3, pp. 421 -430.

Hu, Y.P., Li, Y.R. and Wu, C.M. (2016), "Aspect ratio dependence of Rayleigh-Benard convection of cold water near its density maximum in vertical cylindrical containers", *International Journal of Heat and Mass Transfer*, Vol. 97, pp. 932-942.

Joshi, M.V., Gaitonde, U.N. and Mitra, S.K. (2006), "Analytical study of natural convection in a cavity with volumetric heat generation", *Journal of Heat Transfer*, Vol. 128 No. 2, pp. 176-182.

Khelifi-Touhami, M., Benbrik, A., Lemonnier, D. and Blay, D. (2010), "Laminar natural convection flow in a cylindrical cavity application to the storage of LNG", *Journal of Petroleum Science and Engineering*, Vol. 71 Nos 3/4, pp. 126-132.

Knupp, D.C., Cotta, R.M. and Naveira-Cotta, C.P. (2015a), "Fluid flow and conjugated heat transfer in arbitrarily shaped channels via single domain formulation and integral transforms", *International Journal of Heat and Mass Transfer*, Vol. 82, pp. 479-489.

Knupp, D.C., Naveira-Cotta, C.P. and Cotta, R.M. (2014), "Theoretical-experimental analysis of conjugated heat transfer in nanocomposite heat spreaders with multiple microchannels", *International Journal of Heat and Mass Transfer*, Vol. 74, pp. 306-318.

Knupp, D.C., Naveiracotta, C.P., Renfer, A., Tiwari, M.K., Cotta, R.M. and Poulikakos, D. (2015b), "Analysis of conjugated heat transfer in micro-heat exchangers via integral transforms and non-intrusive optical techniques", *International Journal of Numerical Methods for Heat & Fluid Flow*, Vol. 25 No. 6, pp. 1444-1462.

Leal, M.A., Machado, H.A. and Cotta, R.M. (2000), "Integral transform solutions of transient natural convection in enclosures with variable fluid properties", *International Journal of Heat and Mass Transfer*, Vol. 43 No. 21, pp. 3977-3990.

Leal, M.A., Perez-Guerrero, J.S. and Cotta, R.M. (1999), "Natural convection inside two-dimensional cavities: the integral transform method", *Communications in Numerical Methods in Engineering*, Vol. 15 No. 2, pp. 113-125.

Leong, S.S. (2002), "Numerical study of Rayleigh-Benard convection in a cylinder", *Numerical Heat Transfer Part a-Applications*, Vol. 41 Nos 6/7, pp. 673-683.

Li, Y.H., Chu, T.C. and Lin, T.F. (1996), "Numerical simulation of flow pattern formation in a bottom heated cylindrical fluid layer", *Numerical Heat Transfer Part a-Applications*, Vol. 30 No. 5, pp. 459-476.

Lima, J.A., PerezGuerrero, J.S. and Cotta, R.M. (1997), "Hybrid solution of the averaged navier-stokes equations for turbulent flow", *Computational Mechanics*, Vol. 19 No. 4, pp. 297-307.

Martin, B.W. (1967), "Free convection in a vertical cylinder with internal heat generation", *Proceedings of the Royal Society of London Series a-Mathematical and Physical Sciences*, Vol. 301 No. 1466, pp. 327-341.

Monteiro, E.R., Macedo, E.N., Quaresma, J.N.N. and Cotta, R.M. (2009), "Integral transform solution for hyperbolic heat conduction in a finite slab", *International Communications in Heat and Mass Transfer*, Vol. 36 No. 4, pp. 297-303.

Monteiro, E.R., Macedo, E.N., Quaresma, J.N.N. and Cotta, R.M. (2010), "Laminar flow and convective heat transfer of non-Newtonian fluids in doubly connected ducts", *International Journal of Heat and Mass Transfer*, Vol. 53 No. 11-12, pp. 2434-2448.

Neto, H.L., Quaresma, J.N.N. and Cotta, R.M. (2006), "Integral transform solution for natural convection in three-dimensional porous cavities: aspect ratio effects", *International Journal of Heat and Mass Transfer*, Vol. 49 Nos 23/24, pp. 4687-4695.

Nogueira, E. and Cotta, R.M. (1990), "Heat transfer solutions in laminar co-current flow of immiscible liquids", *Wärme - Und Stoffübertragung*, Vol. 25 No. 6, pp. 361-367.

Oh, J.Y., Ha, M.Y. and Kim, K.C. (1997), "Numerical study of heat transfer and flow of natural convection in an enclosure with a heat-generating conducting body", *Numerical Heat Transfer Part a-Applications*, Vol. 31 No. 3, pp. 289-303.

Paz, S.P.A., Macedo, E.N., Quaresma, J.N.N. and Cotta, R.M. (2007), "Eigenfunction expansion solution for boundary-layer equations in cylindrical coordinates: simultaneously developing flow in circular tubes", *Numerical Heat Transfer Part A Applications*, Vol. 52 No. 12, pp. 1123-1149.

Pereira, L.M., Cotta, R.M. and Guerrero, J.S.P. (2000), "Analysis of laminar forced convection in annular ducts using integral transforms", *Hybrid Methods in Engineering*, Vol. 2 No. 2, pp. 221-232.

Pereira, L.M., Pérez-Guerrero, J.S. and Cotta, R.M. (1998), "Integral transformation of the Navier-Stokes equations in cylindrical geometry", *Computational Mechanics*, Vol. 21 No. 1, pp. 60-70.

Pontedeiro, A.C., Cotta, R.M. and Su, J. (2008), "Improved lumped model for thermal analysis of high burn-up nuclear fuel rods", *Progress in Nuclear Energy*, Vol. 50 No. 7, pp. 767-773.

Rahman, M. and Sharif, M.A.R. (2003), "Numerical study of laminar natural convection in inclined rectangular enclosures of various aspect ratios", *Numerical Heat Transfer Part a-Applications*, Vol. 44 No. 4, pp. 355-373.

Roh, S., Son, G., Song, G. and Bae, J. (2013), "Numerical study of transient natural convection in a pressurized LNG storage tank", *Applied Thermal Engineering*, Vol. 52 No. 1, pp. 209-220.

Silva, C.A.M., Macedo, E.N., Quaresma, J.N.N., Pereira, L.M. and Cotta, R.M. (2010), "Integral transform solution of the navier-stokes equations in full cylindrical regions with streamfunction formulation", *International Journal for Numerical Methods in Biomedical Engineering*, Vol. 26 No. 11, pp. 1417-1434.

Wang, B.F., Ma, D.J., Guo, Z.W. and Sun, D.J. (2014), "Linear instability analysis of Rayleigh-Benard convection in a cylinder with traveling magnetic field", *Journal of Crystal Growth*, Vol. 400, pp. 49-53.

Wang, B.F., Zhou, L., Jiang, J. and Sun, D.J. (2016), "Numerical investigation of Rayleigh-Benard convection in a cylinder of unit aspect ratio", *Fluid Dynamics Research*, Vol. 48 No. 1.

Wolfram, S. (2003), *The Mathematica Book*, 5th ed., Wolfram Media/Cambridge University Press, Champaign, IL.

Corresponding author
Guangming Fu can be contacted at: fu@upc.edu.cn